BNL-229585-2026-TECH

EIC-ADD-TN-162

Estimation of radiation fields generated by injected beam losses at the EIC's RCS

R. dos Santos Augusto

March 2026

Electron-Ion Collider

Brookhaven National Laboratory

U.S. Department of Energy

USDOE Office of Science (SC), Nuclear Physics (NP)

DISCLAIMER

Estimation of radiation fields generated by injected beam losses at the EIC's RCS

R. S. Augusto*, J. P. Saraiva, and C. W. Schaefer
Brookhaven National Laboratory, Upton, NY 11973-5000.

(Dated: March 5, 2026)

This technical note provides a general estimate of radiation fields generated by injection fault events at the electron-ion collider´s (EIC) Rapid Cycling Synchrotron (RCS), calculated with the Monte Carlo particle transport and interaction code FLUKA. Calculations were performed for two major injection loss scenarios that involve iron targets and featured different electron beam energy and current values. The results presented here constitute a first order assessment of several radiological quantities associated with these electromagnetic showers and their potential effect on environmental safety and health (ESH) systems in the vicinity of injection areas.

ACRONYMS

BNL Brookhaven National Laboratory
EIC Electron-Ion Collider
ESH Environmental Safety and Health
ESR Electron Storage Ring
FLUKA FLUktuierende KAskade Monte Carlo particle transport and interaction code
HEH High Energy Hadron equivalent estimator
LHC Large Hadron Collider
LINAC Linear Accelerator
MC Monte Carlo (method)
NIEL Non-ionizing Energy Losses
RCS Rapid Cycling Synchrotron
RHIC Relativistic Heavy Ion Collider
SEU Single Event Upset

CONTENTS

*rdossanto@bnl.gov

I. INTRODUCTION

The Electron-Ion Collider (EIC) is currently under construction at Brookhaven National Laboratory (BNL), in partnership with Thomas Jefferson National Accelerator Facility (Jefferson Lab). When operational, EIC will generate events from $e + p$ and $e + A$ collisions in a high luminosity regime and a center-of-mass energy of up to 141 GeV, for 18 GeV electron collisions with protons at up to 275 GeV [1–3]. For heavier ions such as gold, the ion beam energy will reach up to 100 GeV per nucleon and thus the center-of-mass energy may attain 85 GeV per nucleon depending on the operating electron beam energy.

While the EIC will repurpose one of the extant Relativistic Heavy Ion Collider's (RHIC) rings for storing its hadrons, RHIC's second ring will have to be converted into a dedicated Electron Storage Ring (ESR) [4]. This new ring will need to be capable to provide polarized electron beams at three different energies (5, 10, and 18 GeV) for the collisions with hadrons in the ePIC Detector point, as depicted in figure 1 [5].

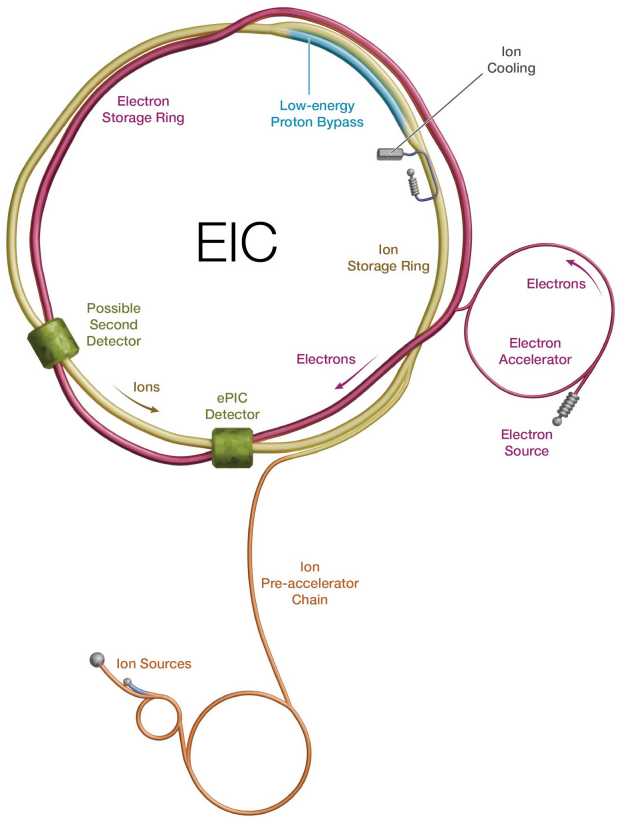

FIG. 1. *The EIC accelerator chain and major components as of March 2025. The electron beam travels in the red segments, starting from the electron source, then it is accelerated by a* LINAC *and then the RCS (small ring on the right side) before being delivered into the ESR. Source:* https://www.bnl.gov/eic/machine.php

The precision measurements of these interactions will provide valuable insight into the nuclear structure and subatomic landscape of matter, helping to understand how quarks and gluons are arranged, interact, and give rise to the basic physical properties of protons and neutrons, potentially answering various fundamental physics questions [6, 7].

As part of the newly designed electron injection complex, electrons are delivered into the ESR at full energy from a Rapid Cycling Synchrotron (RCS), where electron charge is accumulated into a single bunch at a rate of up to 28 $\mathrm{nC\,s^{-1}}$ [5]. Given the relatively high electron beam power in these bunches, injection losses in the RCS need to be properly assessed and their radiological impact quantified and mitigated as needed. Moreover, whilst the impact of ion injection losses may be somewhat extrapolated from RHIC's operation history, the same does not apply to injection electron losses due to the completely different physics mechanisms.

II. METHODOLOGY

In this work, the Monte Carlo (MC) particle transport and interaction code FLUKA (http://www.fluka.eu) [8, 9] is used to characterize the showers resulting from crudely defined electron beam injection losses. The main objective is to determine the radiation dose associated with the operation of different electron beam energies and assess their potential impact on environmental safety and health (ESH) systems near the beamline, which should not be exposed to radiation levels greater than 50 rem $\mathrm{h^{-1}}$ [10]. Two radiation damage estimators were also tallied, to complement the dosimetry data obtained.

No effort was made to replicate the actual geometry of the RCS, nor the complex beam dynamics that may describe an injection fault event with the utmost accuracy. These effects can be particularly important for determining the radiological impact on specific components of the beamline, and will likely be extensively evaluated via precise beam-machine protection assessments as design progresses. Instead, this work intends to provide a general estimate of the radiation fields in close proximity to an injection fault event by assuming only a bare geometry, and to provide guidance on what minimum distance from the beamline should be kept for these ESH systems.

It should be stressed that there will also be other sources of radiation in the RCS in addition to the electron beam injection losses simulated in this work. Thus, it is highly recommended to characterize the anticipated chronic mixed radiation field to validate whether its proposed location is appropriate and confirm what type of technology should be used, possible shielding requirements, and expected operating lifetime.

III. SIMULATION DETAILS

The FLUKA simulations consisted mainly of the reproduction of two injection fault scenarios – grazing incidence ($\mathcal{G}$) and normal incidence ($\mathcal{Z}$) – on iron targets, as detailed in figure 2.

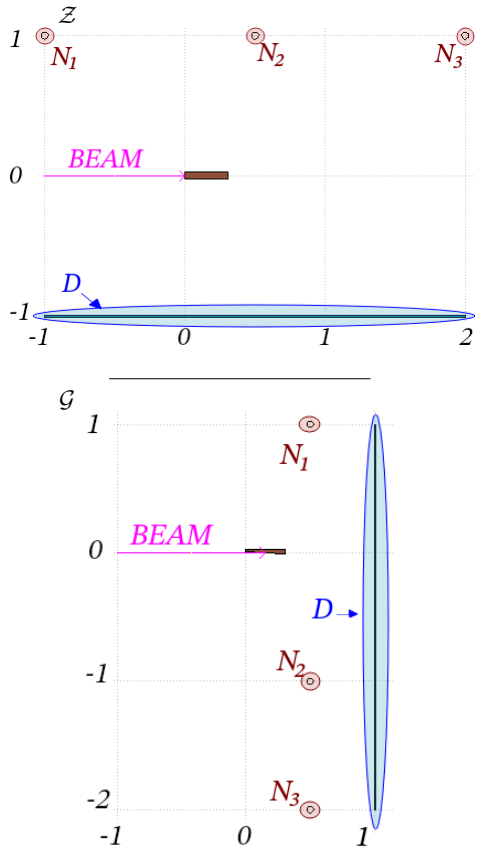

FIG. 2. *Schematic depictions of the electron beam loss scenarios - normal incidence in the upper panel and grazing incidence on the bottom panel - based on the flair geoviewer visualization [11]. The location of neutron detectors (N) are indicated and the dosimetry scoring detector (D) highlighted. All values are given in meters.*

These scenarios can be described as:

- $\mathcal{G}$ - electron beam consisted of a squared beam with 1 cm^2 cross sectional area, shaving an Fe target with a gradual loss over the 12 inches (30.48 cm) length of the target.
- $\mathcal{Z}$ - a pencil electron beam impinges directly onto a cylindrical iron block 30.48 cm long and with 5 cm diameter.

Three energy variants for each scenario were considered, corresponding to 5, 10, or 18 GeV electron beam's kinetic energy and specific current parameters associated with each energy operation [10]. The values are listed in table I

TABLE I. *Beam energy and intensity parameters used for the variants in each of the scenarios $\mathcal{G}$ and $\mathcal{Z}$.*

Variant	$(\mathcal{G} \mid \mathcal{Z})_1$	$(\mathcal{G} \mid \mathcal{Z})_2$	$(\mathcal{G} \mid \mathcal{Z})_3$
Electron beam energy [GeV]	*5*	*10*	*18*
Injected beam intensity [nA]	*28*	*28*	*11*

In each of the scenarios, virtual spherical neutron detectors were placed in the locations indicated as $N_{1,2,3}$ in figure 2, and incoming spectra were collected therein via `USRBDX`. The extension denoted as "D" refers to a virtual detector, consisting of a long and thin line, where absorbed dose and ambient dose are tallied with `USRBIN` in steps of 1 cm.

Regarding the FLUKA estimators for assessing the radiation damage inducing effects, Si 1 MeV-neutron equivalent fluence and high energy hadron (HEH) equivalent fluence were chosen to complement the dosimetry data obtained for each scenario. The 1 MeV-neutron equivalent fluence in silicon is a standard quantity for normalizing displacement damage in silicon detectors and electronics from an arbitrary radiation field with a given energy spectrum to an equivalent damage level produced by 1 MeV neutrons. It specifically quantifies non-ionizing energy loss (NIEL) and displacement damage in silicon. As for the HEH equivalent fluence, it is proportional to the number of Single Event Upsets (SEU's) due to hadrons with energy over 20 MeV. It should be noted that unstable hadrons of lower energies as well as low energy neutrons are also factored in the estimator [12]. These quantities are relevant mainly for electronic systems, and hence helpful to inform how detrimental some components of the mixed radiation field can be to specific devices based on their reference damage values or error data.

IV. RESULTS

The ambient dose rate maps pertaining to the scenarios $\mathcal{Z}$ and $\mathcal{G}$ can be found in figures 3 and 4, respectively.

A direct comparison between ambient dose and absorbed dose rates in each scenario is given in figure 5, as scored in the virtual detector "D".

From all scenarios and variants considered, the maximal electromagnetic (photon and electron/positron) and neutronic fluence maps are presented in figure 6.

The neutron fluence spectra are shown in figure 7. It features a comparison between the two scenarios, at the worst case location (N_2 in figure 2), followed subsequently by an inter-comparison between the three energy variants for that most conservative neutronic scenario ($\mathcal{Z}$).

The radiation damage estimators, corresponding to the HEH and Si 1 MeV-neutron equivalent fluence, are also provided in figure 8 for the most conservative case scored (i.e., $\mathcal{G}_2$).

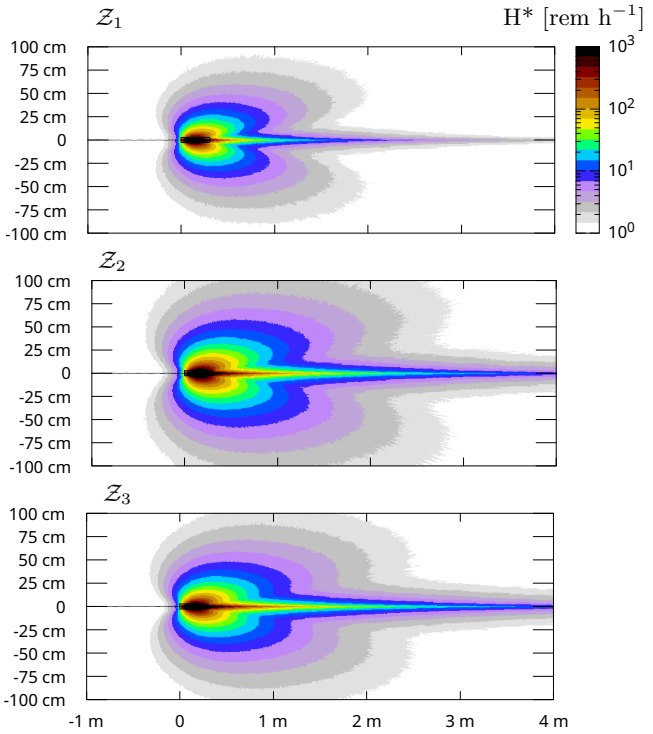

FIG. 3. *Ambient dose rates (H*) distribution for the energy variants of scenario $\mathcal{Z}$. The results are averaged over 2* cm*, centered at the beam elevation.*

V. DISCUSSION

The ambient dose maps shown in figures 3 and 4 denote maximum radiation levels for the 10 GeV cases. This is because of the difference in intensity between the 10 GeV and 18 GeV variants, of almost a factor 2.5, whereas the difference in energy is less than a factor of two. Overall, the radiation levels for the 10 GeV case tends to be 40% higher than the 18 GeV, and almost twice that of 5 GeV, which tends to align well with the power difference between cases.

Radiation levels for the 10 GeV injection loss reach 50 rem h^{-1} at about 20 cm laterally from the loss point (see figure 3) in scenario $\mathcal{Z}$, whereas for scenario $\mathcal{G}$ 50 rem h^{-1} are reached at about 50 cm downstream and laterally from the loss point as depicted in figure 4.

It is clear that radiation levels could be much higher directly downstream of the target for a grazing incident, depending on the amount and shape of material traversed (and its composition). Even slight angular variations of scenario $\mathcal{G}$ can induce electromagnetic showers that have the capacity to propagate several meters farther downstream and scatter throughout the various beamline components, potentially generating radiation fields higher than those denoted in figure 4.

Figure 5 quantifies the absorbed dose and ambient dose rates for each scenario at a virtual detector (D in figure 2). These confirm that laterally, at about 1 m distance from the target, the H* values do not exceed the 2.5 rem h^{-1} in scenario $\mathcal{Z}$ with absorbed doses reaching at most 0.3 rad h^{-1}. Conversely, for scenario $\mathcal{G}$, the downstream detector captures the particle shower resulting from the interaction with the target, denoting stark dosimetry variations as expected from figure 4. In particular, for the inboard side of the 10 GeV fault, the absorbed doses can range from 3–30 rad h^{-1} between 2 and 1 m distance laterally from the target.

In every energy variant, directly downstream of the target, the absorbed doses can reach several hundreds of rad h^{-1} (and about one order magnitude greater in the case of H*), which underscores the importance of limiting the angular acceptance of injection losses to mitigate their radiological impact in the beamline's vicinity. If injection faults can indeed occur at large angles, placement of systems farther laterally from a known loss point could be ineffective at preventing unwarranted exposure to dose rates above one gray hourly. In the latter case, placing the ESH systems far from the injection points or provide them with local shielding could be the only valid alternative.

The electron beam interactions with iron targets generate showers that are almost entirely dominated by electromagnetic particles whose fluence is maximal for $\mathcal{G}_2$, due to the higher power and grazing interaction, as illustrated in figure 6. There is also a significant production of neutrons, particularly in the $\mathcal{Z}_2$ scenario due to the sheer amount of beam particles interacting with the target – see figure 7. However, as it can be observed from figure 6, lateral neutron fluences are almost three orders of magnitude lower than electromagnetic particle fluences at similar distance. The vast majority of these neutrons derive from photonuclear interactions of the shower photons, with only a very small portion of the neutrons being directly attributed to electronuclear interactions. An important component of the neutron spectra lies in the secondary hadronic cascades, which becomes increasingly relevant for the higher energy cases as this hadronic component promotes spallation reactions in iron, incrementing the harder component of the neutron spectrum. Note that neutron production is also relatively dependent on the material type, and hence neutron fluence values will differ for a non-ferrous target.

Regarding the radiation damage estimators, the highest fluence rates corresponded to scenario $\mathcal{G}_2$ for both estimators depicted in figure 8. The HEH equivalent fluence attains over 10^5 cm^{-2} per injection loss event at one meter from the target, which is close to the annual HEH fluence at sea level [13]. Similarly, the silicon 1 MeV-neutron equivalent fluence does not exceed 10^8 cm^{-2} at half metre laterally from the target, well below the 10^{11} cm^{-2} fluence threshold in which earlier damage starts occurring [14]. For guidance, the effects from a 10^{10} cm^{-2} Si 1 MeV-neutron equivalent fluence are considered to be comparable to 100 rad (Si) in the LHC context [13].

These results are relatively benign for a single injection loss event, and hence could only become problematic in cumulative terms, for instance if frequent (hundreds) of

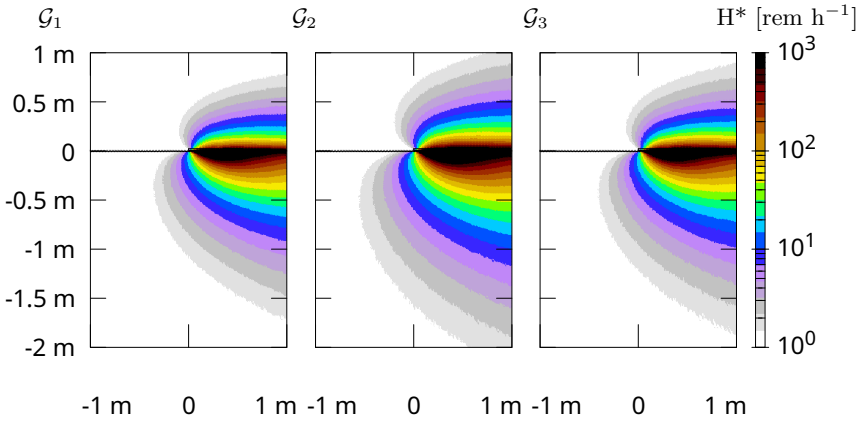

FIG. 4. *Ambient dose rate (H*) distribution for the energy variants of scenario $\mathcal{G}$. The results are averaged over 2* cm*, centered at the beam elevation.*

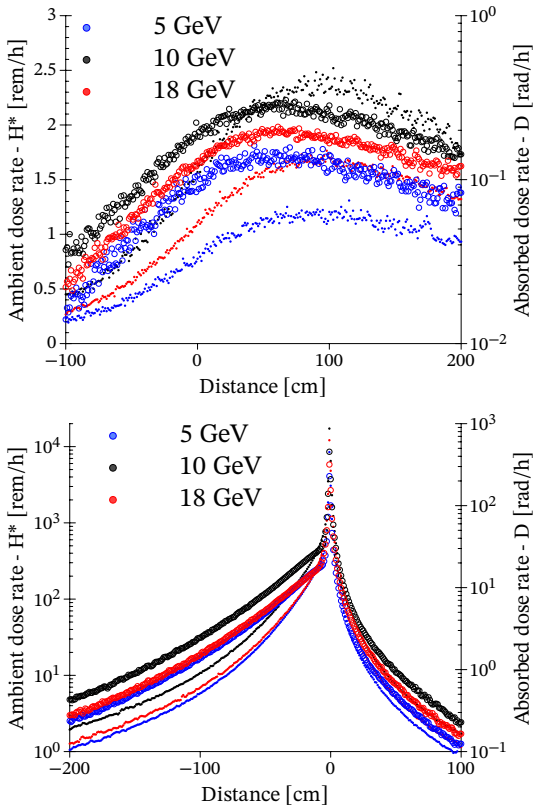

FIG. 5. *Ambient dose (closed circles) and absorbed dose (open circles) rates calculated in the detector "D" for each electron beam energy. The upper panel refer to scenario $\mathcal{Z}$ whereas the lower panel refers to scenario $\mathcal{G}$.*

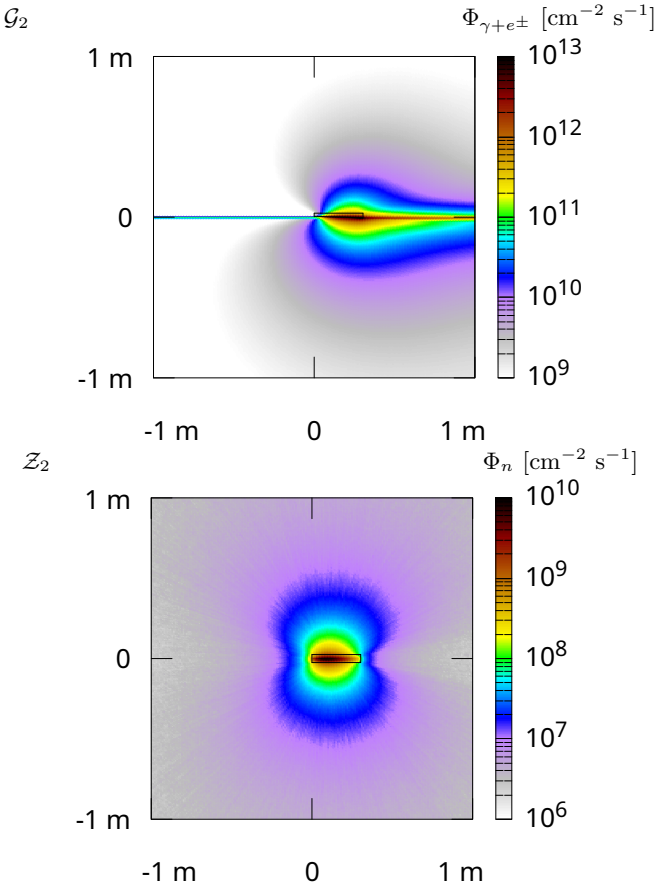

FIG. 6. *Upper panel – electromagnetic (γ+$e^\pm$) particle fluence rates in scenario $\mathcal{G}_2$; Bottom panel – neutron fluence rates in scenario $\mathcal{Z}_2$; these correspond to the highest rate for the respective particle fluence type. Note the different color band scale. The results are averaged over 2* cm*, centered at the beam elevation.*

such injection losses take place in a year affecting the same location. Nevertheless, irrespective of the damage thresholds, the actual system failures will always depend chiefly on the component technology, their size, and the nature of the radiation source term (e.g., whether it is partially shielded or fully exposed to a loss point).

The characterization of the overall mixed field radiation environment at the expected ESH system location in the tunnel is most important to properly interpret this study's results. While dose rates derived from injection

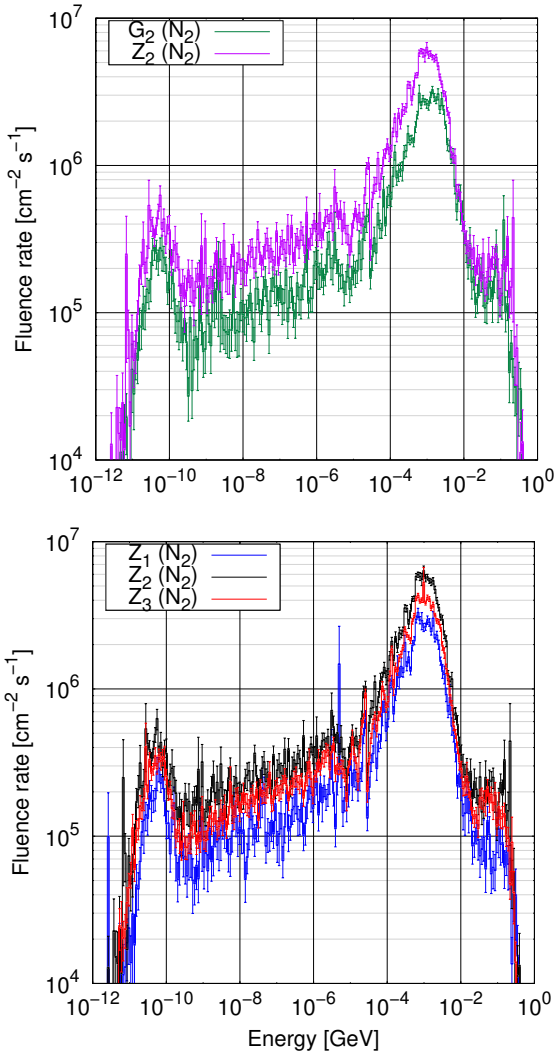

FIG. 7. *Upper panel – Comparison of neutron spectra scored in the N_2 for scenarios $\mathcal{Z}_2$ and $\mathcal{G}_2$. Bottom panel – For scenario $\mathcal{Z}$, the neutron spectra scored in the detector N_2 are displayed for each beam energy.*

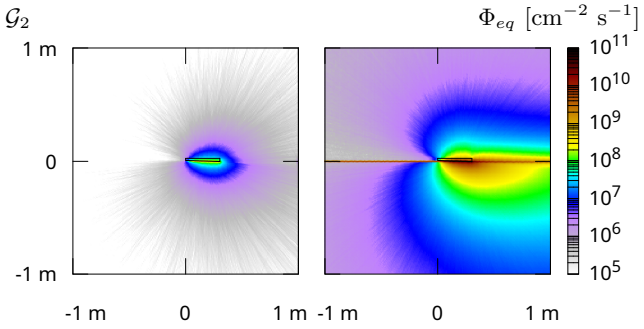

FIG. 8. *Equivalent fluence rates of HEH (left) and silicon 1 MeV-neutron (right) estimators for the scenario $\mathcal{G}_2$. The results are averaged over 2* cm*, centered at the beam elevation.*

faults may likely dominate the radiation fields punctually due to their magnitude, the combined effect of chronic sources of radiation (e.g., Synchrotron Radiation, Gas Bremsstrahlung) might become relevant over time if unmitigated. The same applies to neutrons, HEH and Si 1 MeV-neutron equivalent fluences, which may be underestimated since the cumulative contribution from chronic beam losses are not being accounted for in this work. Final validation of the detector locations should therefore include sources of radiation beyond injection faults.

VI. CONCLUSION

Injection electron beam losses at the RCS were characterized for a simplified normal and grazing incidence fault scenario, each at three different energy and intensity regimes.

It was confirmed that the highest power source term at 10 GeV was also the most conservative from a dosimetry standpoint. For this worst case scenario, radiation levels could attain 50 rem h^{-1} at about 50 cm laterally from an iron target in the grazing incidence scenario whereas for normal incidence the same dose could be obtained at 20 cm laterally from the target. Generally absorbed doses were found to be one order magnitude lower than ambient dosage. Due to the nature of the beam-matter interaction and the electromagnetic shower development, dose rates could be much higher in the path downstream of the loss point, requiring further studies with an accurate geometry in case ESH systems need to be placed in close proximity to the beamline.

The neutron fluence were observed to be far lower than the electromagnetic particles fluence, even for a loss at normal incidence, as expected due to the former's indirect production channels. Furthermore, radiation damage estimators such as Si 1 MeV-neutron equivalent and HEH equivalent fluence were found to be relatively low, which might be encouraging for systems relying on non-hardenened electronics and assuming that the fault scenarios will be rather infrequent. However, this analysis neglected the contribution from chronic sources of radiation in the RCS, and only if these cumulative contributions are taken into account the radiological impact to ESH systems can be fully determined.

ACKNOWLEDGMENTS

The authors wish to thank the National Synchrotron Light Source II's Environment Safety and Health group for providing the computational resources for the radiation transport calculations in this work.

This work was supported by Environment Safety and Health group of EIC. The EIC project is a partnership between Brookhaven National Laboratory and Thomas Jefferson National Accelerator Facility and is funded by the U. S. Department of Energy (DOE) Office of Science.

[1] J. Jiménez-López, P. R. Newman, and K. Wichmann, Prospects for measurements of the longitudinal proton structure function F_L at the electron ion collider, Phys. Rev. D **111**, 056014 (2025).

[2] A. Seryi et al, The US Electron Ion Collider Accelerator Designs, in *Proc. NAPAC'19*, North American Particle Accelerator Conference No. 4 (JACoW Publishing, Geneva, Switzerland, 2019) pp. 1–7, https://-doi.org/10.18429/JACoW-NAPAC2019-MOOHC2.

[3] F. Willeke, Design of the Electron-Ion Collider, *Acta Physica Polonica B Proceedings Supplement* ***16***, 7-A1 *(2023).*

[4] F. Willeke et al., Electron Ion Collider Conceptual Design Report 2021*, Tech. Rep. BNL-221006-2021-FORE (Brookhaven National Laboratory, 2021).*

[5] G. Atoian et al, Realizing the scientific program with polarized ion beams at eic (2025), arXiv:2510.10794 [nucl-ex].

[6] R. Abdul Khalek et al , Science requirements and detector concepts for the electron-ion collider, Nuclear Physics A ***1026****, 122447 (2022).*

[7] A. Accardi et al., Electron Ion Collider: The Next QCD Frontier - Understanding the glue that binds us all (2014), arXiv:1212.1701 [nucl-ex].

[8] A. Ferrari, P. R. Sala, A. Fassò, and J. Ranft, FLUKA: a multi-particle transport code *(2005), CERN-2005-10, INFN/TC_05/11, SLAC-R-773.*

[9] F. Ballarini et al. (The FLUKA Collaboration), The FLUKA code: Overview and new developments, EPJ Nuclear Sci. Technol. ***10****, 16 (2024).*

[10] C. W. Schaefer, personal communication (2026).

[11] V.Vlachoudis, Flair*: A Powerful But User Friendly Graphical Interface For FLUKA, Proc. Int. Conf. on Mathematics, Computational Methods Reactor Physics (MC 2009), Saratoga Springs, New York, 2009 (2009).*

[12] A. Ferrari, P. Sala, A. Fassò, and J. Ranft, FLUKA: A Multi-Particle Transport Code — Manual*, The FLUKA Collaboration (2025).*

[13] R. García Alía, M. Brugger, S. Danzeca, F. Cerutti, J. P. de Carvalho Saraiva, R. Denz, A. Ferrari, L. L. Foro, P. Peronnard, K. Røed, R. Secondo, J. Steckert, Y. Thurel, I. Toccafondo, and S. Uznanski, Single event effects in high-energy accelerators, Semiconductor Science and Technology ***32****, 034003 (2017).*

[14] M. Moll, E. Fretwurst, and G. Lindström, Leakage current of hadron irradiated silicon detectors — material dependence, Nuclear Instruments and Methods in Physics Research A ***426****, 87 (1999).*